

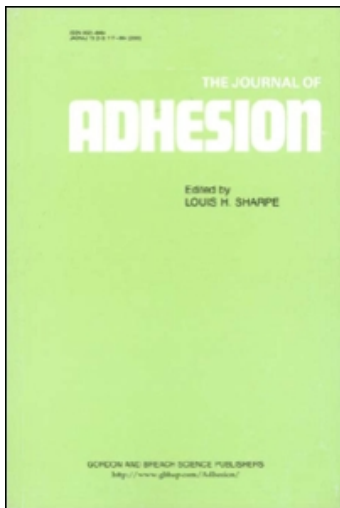
This article was downloaded by:

On: 22 January 2011

Access details: *Access Details: Free Access*

Publisher *Taylor & Francis*

Informa Ltd Registered in England and Wales Registered Number: 1072954 Registered office: Mortimer House, 37-41 Mortimer Street, London W1T 3JH, UK



The Journal of Adhesion

Publication details, including instructions for authors and subscription information:

<http://www.informaworld.com/smpp/title~content=t713453635>

Surface Characterization of Plasma Treated Carbon Fibers and Adhesion to a Thermoplastic Polymer

P. Commerçon^a; J. P. Wightman^a

^a Chemistry Department, Virginia Institute for Material Systems, Virginia Polytechnic Institute and State University, Blacksburg, VA, USA

To cite this Article Commerçon, P. and Wightman, J. P.(1992) 'Surface Characterization of Plasma Treated Carbon Fibers and Adhesion to a Thermoplastic Polymer', *The Journal of Adhesion*, 38: 1, 55 – 78

To link to this Article: DOI: 10.1080/00218469208031267

URL: <http://dx.doi.org/10.1080/00218469208031267>

PLEASE SCROLL DOWN FOR ARTICLE

Full terms and conditions of use: <http://www.informaworld.com/terms-and-conditions-of-access.pdf>

This article may be used for research, teaching and private study purposes. Any substantial or systematic reproduction, re-distribution, re-selling, loan or sub-licensing, systematic supply or distribution in any form to anyone is expressly forbidden.

The publisher does not give any warranty express or implied or make any representation that the contents will be complete or accurate or up to date. The accuracy of any instructions, formulae and drug doses should be independently verified with primary sources. The publisher shall not be liable for any loss, actions, claims, proceedings, demand or costs or damages whatsoever or howsoever caused arising directly or indirectly in connection with or arising out of the use of this material.

Surface Characterization of Plasma Treated Carbon Fibers and Adhesion to a Thermoplastic Polymer

P. COMMERÇON and J. P. WIGHTMAN

Chemistry Department, Virginia Institute for Material Systems, Virginia Polytechnic Institute and State University, Blacksburg, VA 24061, USA

(Received June 7, 1991; in final form January 28, 1992)

The surface chemistry of IM7 carbon fibers was characterized by x-ray photoelectron spectroscopy (XPS). The fiber surface energetics were determined from a two-liquid tensiometric method. The adhesion between as-received and plasma-treated carbon fibers and polyethersulfone (PES) was measured by the microbond pull-out test.

The surface characterization techniques showed that the effect of any plasma treatment is attained within less than 15 seconds. It was found that both argon and air plasmas increased the oxidation state of the fiber surface and that they reduced the dispersive component (γ_s^d) of the fiber surface free energy considerably. The ammonia plasma treatment resulted in a cleaning of the surface. This plasma treatment was also effective in improving the fiber/matrix adhesion of quenched samples. A similar adhesion enhancement between as-received fibers and PES is obtained by annealing the samples above the T_g of the polymer. The air plasma treatment did not have any significant effect on the fiber/matrix adhesion.

KEY WORDS Carbon fibers; plasma treatment; fiber-matrix adhesion; thermoplastic matrix; microbond pull-out test; dynamic contact angle; x-ray photoelectron spectroscopy.

INTRODUCTION

The understanding of the fiber-matrix interaction is of fundamental importance in the design of new fiber reinforced plastics. The interphase between the two components plays a key role in the overall mechanical properties of the composite through load transfer mechanisms. Historically the emphasis has been put on epoxy matrix structural composites and numerous studies have been published. The development of engineering thermoplastics, which are tougher than epoxides, and exhibit better chemical resistance, opens the way to a new family of high-performance composites. In addition to their interesting intrinsic mechanical, thermal and chemical properties, these polymers, when used as matrices in composites, have processing advantages such as short cycles, scrap recovery and indefinite shelf-life.¹ But thermoplastic matrix/carbon fiber interactions have not been as well documented as those in epoxy-matrix composites.

There are numerous ways to modify the surface chemistry and the surface ener-

getics of carbon fibers.² But the development of air-to-air plasma equipment raises new interest in plasmas as fiber surface pretreatments. Plasmas have been used to increase the polarity^{2,3} and to introduce specific functional groups on the surface of carbon fibers.⁴⁻⁶ Fibers with high surface energy are more readily wetted by the matrix polymer and stronger adhesion between the fibers and the polymer is expected. Surface treatments can also affect the fiber acidity, as measured by inverse gas chromatography (IGC) and, therefore, the adhesion between acidic carbon fibers and basic thermoplastics.^{7,8}

The purpose of this work is to study the influence of plasma treatments of the surface of reinforcing carbon fibers on the adhesion between the fibers and a thermoplastic resin.

BACKGROUND

Dynamic Contact Angle: Two-Liquid Method

The two-liquid method has been used by Donnet and Schultz to measure the dispersive component of the surface energy of cleaved muscovite mica.⁹⁻¹¹ In this technique a high surface energy solid is immersed in a nonpolar solvent, usually a linear alkane. The advantage of this method is that a polar liquid such as water or formamide, immiscible with the hydrocarbon, gives a non-zero contact angle. The technique was adapted to surface energy characterization studies of small diameter fibers.^{12,13} Figure 1 shows a schematic diagram of a fiber immersed in two immiscible liquids L1 and L2.

Assuming that the equilibrium spreading pressure π_e is negligible so that $\gamma_s = \gamma_{sv}$ the expression of the work of adhesion at the first interface (fiber/L1/air) can be written as:

$$W_{al} = \gamma_s + \gamma_1 - \gamma_{s1} = 2[\gamma_s^d \gamma_1^d]^{1/2} \quad (1)$$

$$\Leftrightarrow \gamma_s = \gamma_{s1} - \gamma_1 + 2[\gamma_s^d \gamma_1^d]^{1/2} \quad (1a)$$

since there are no non-dispersive interactions.

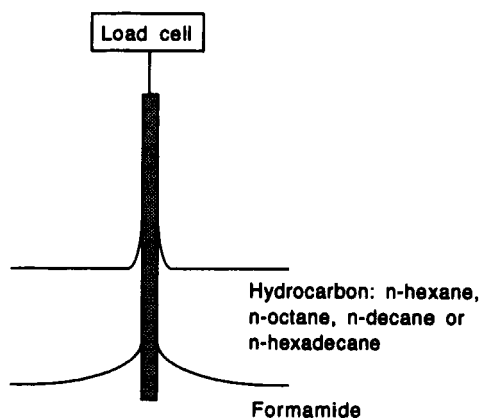


FIGURE 1 Schematic diagram of the fiber/L1/air and fiber/L1/L2 interfaces. L1-Hydrocarbon; L2-Formamide

γ_s , γ_s^d , γ_1 and γ_1^d are the surface free energies, and their dispersive component, of the fiber and the liquid L1, respectively. γ_{s1} is the interfacial surface tension between the fiber and the liquid L1. At the second interface (fiber/L1/L2) Young's equation and the work of adhesion can be written as:

Young's equation:

$$\gamma_{s1} = \gamma_{s2} + \gamma_{12} \cos(\theta_{s2/1}) \quad (2)$$

which can be rearranged into:

$$\gamma_{s2} = \gamma_{s1} - \gamma_{12} \cos(\theta_{s2/1}) \quad (2a)$$

and

$$W_{a2} = \gamma_s + \gamma_2 - \gamma_{s2} = 2[\gamma_s^d \gamma_2^d]^{1/2} + I_{s2}^p \quad (3)$$

Substituting (1a) and (2a) into (3) and rearranging leads to

$$\gamma_2 - \gamma_1 + \gamma_{12} \cos(\theta_{s2/1}) = 2(\gamma_s^d)^{1/2} [(\gamma_2^d)^{1/2} - (\gamma_1^d)^{1/2}] + I_{s2}^p \quad (4)$$

γ_2 and γ_2^d are the surface free energy, and its dispersive component, of the liquid L2. γ_{12} is the interfacial surface tension between the two liquids. $\theta_{s2/1}$ is the contact angle at the triple phase line. I_{s2}^p is the contribution to the work of adhesion, W_{a2} , which accounts for all the non-dispersive interactions.

If the liquid L1 is a hydrocarbon (suffix "H") and L2 is formamide (suffix "F"), equation (4) takes the final form:

$$\gamma_F - \gamma_H + T = 2(\gamma_s^d)^{1/2} [(\gamma_F^d)^{1/2} - (\gamma_H^d)^{1/2}] + I_{sF}^p \quad (5)$$

where $\gamma_H = \gamma_H^d$ for hydrocarbons.

$$T = \gamma_{HF} \cos \theta_{S F/H} = \frac{f_{HF}}{f_{HA}} \gamma_H = \frac{f}{C} - \gamma_H \quad (6)$$

and

$$C = \frac{f_{HA}}{\gamma_H} \quad (7)$$

where γ_{HF} is the interfacial surface tension between formamide and the hydrocarbon

C is the circumference of the fiber

f is the net force recorded by the balance

The forces measured by the microbalance are the apparent weight of the liquid raised by capillary forces at the air/hydrocarbon/fiber interface (f_{HA}) and at the hydrocarbon/formamide/fiber interface (f_{HF}). The dispersive component, γ_s^d , is calculated from the slope of the straight line obtained by plotting the left term of equation (5) versus the term in brackets on the right-hand side of this equation. The intercept gives the nondispersive term I_{sF}^p . Equation (5) assumes that the formamide

displaces the hydrocarbon during the immersion of the fiber and that the hydrocarbon displaces the formamide during the emersion stage. The displacement criteria have been derived by Shanahan *et al.*¹⁴ and are reproduced below:

Advancing criterion:

$$I_{SF}^p > 2[(\gamma_s^d)^{1/2} - (\gamma_H)^{1/2}][(\gamma_H)^{1/2} - (\gamma_F^d)^{1/2}] \quad (8)$$

Retreating criterion:

$$I_{SF}^p < 2[\gamma_F^p - [(\gamma_s^d)^{1/2} - (\gamma_F^d)^{1/2}][(\gamma_F^d)^{1/2} - (\gamma_H)^{1/2}]] \quad (9)$$

These criteria are based on the hypotheses that the equilibrium spreading pressure, π_e , of both liquids on the fiber is negligible and that the surface is perfectly homogeneous and smooth.

Microbond Pull-Out Test

In a pull-out test a given amount of resin surrounds a single fiber. The resin bead is slid along the fiber and the interfacial shear strength is calculated by dividing the measured debonding force by the contact area between the fiber and the resin. In order to observe a sliding of the resin along the fiber, the shearing force has to be less than the tensile strength of the fiber, otherwise the fiber breaks first. Therefore, there is a critical contact area (or, for fibers of constant diameter, "d," a critical embedment length, "l_c") for which the shearing force is equal to the tensile strength of the fiber. Thus:

$$\sigma_f \pi d^2 / 4 = \tau \pi d l_c \quad (10)$$

or

$$l_c = (\sigma_f d) / (4 \tau) \quad (11)$$

where τ is the average shear stress along the bonded area

σ_f is the fiber tensile strength or normal stress.

A major problem encountered with this test when using small diameter fibers such as carbon fibers is that the critical length l_c is usually very small. Consequently, it is difficult to make test specimens. Miller and co-workers proposed an original procedure to prepare samples in the case of small fibers.¹⁵⁻¹⁹ The method was first applied to epoxy/glass fibers, epoxy/Kevlar® fibers and epoxy/carbon fibers¹⁵ systems but has also been used for carbon fibers/thermoplastic resins systems¹⁹ and a Kevlar®/polycarbonate system.¹⁸ Stress and force distributions in the microbond pull-out test as well as fatigue behavior have been studied theoretically.^{16,20}

EXPERIMENTAL

The carbon fibers used in this study were unsized IM7, from Hercules. The thermoplastic polymer was polyethersulfone (PES) from ICI, T_g ≈ 220°C by DSC.

Plasma Treatment

A bench top Tegal Plasmod® plasma chamber was used for the surface treatment of the IM7 carbon fibers. The radio frequency (13.56 MHz) generated plasma was operated at 50 W. An oxygen plasma appeared to be too corrosive and completely burned single fibers within a few seconds. Air was substituted for oxygen as the oxidative gas. Argon was chosen as a model for a neutral gas. Ammonia was chosen in order to introduce nitrogen functionalities. A constant reduced pressure (0.1 torr) was maintained during the treatment by a combination of continuous evacuation and gas inlet through a microleak. The fibers were treated for 15, 30, 60 or 120 seconds.

Dynamic Contact Angle Analysis

The surface free energy, γ_s , of as-received carbon fibers was generally greater than 40 mJ/m². For this reason the IM7 carbon fibers have been considered, *a priori*, to be high energy solids and a two-liquid tensiometric technique has been used to measure surface free energy.

A single fiber was attached to a 100 μm diameter wire with a cyanoacrylate adhesive. The wire was suspended from the measuring arm of a Cahn DCA 322 electrobalance. The fiber was immersed in a system consisting of two immiscible liquids: formamide and a hydrocarbon. The less dense alkane formed the top layer, which was the first layer encountered by the fiber. The series of hydrocarbons used were: n-hexane, n-octane, n-decane and n-hexadecane. The beaker containing the liquids rested on a vertical translator. The stage displacement speed was set at 20 $\mu\text{m}/\text{sec}$. The increase in the weight of the fiber observed after immersion was measured by the balance. The data were collected and analyzed by a personal computer. Both advancing and receding curves were recorded.

XPS Analysis

As-received and plasma treated tows of carbon fibers were cut into 2 cm long sections. Three or four of these small bundles were placed on the XPS sample holder. The fibers were maintained in place with an aluminum ring that was screwed onto the sample holder. The fibers were analyzed in a 5400 Perkin Elmer x-ray photoelectron spectrometer. The XPS spectrometer was operated in the fixed analyzer mode with the use of Mg $K\alpha_{1,2}$ x-ray radiation (400 W, 15 kV). The gold 4f7/2 (83.8 eV) and copper 2p3/2 (932.4 eV) peaks were used for the energy calibration of the instrument. The intensity calibration was made on the silver 3d5/2 (367.9 eV) peak, according to the Perkin Elmer standard procedure. The sample holder was oriented at 45° with respect to the analyzer. The collecting time was 5 min. for a wide scan (0–1100 eV) as well as for each narrow scan. The curve fitting program uses a weighted least squares fit with integrated background and a Gaussian function. The full width at half maximum (FWHM) was kept constant for all curve fittings with the following values: FWHM = 1.5 eV for the main graphitic peak, FWHM = 1.6 eV for the functionalized carbon peaks, and finally FWHM = 1.7–1.8 eV for the $\pi \rightarrow \pi^*$ shake-up satellite peak.

Surface Morphology

SEM micrographs of the surface morphology of the fibers were obtained from a ISI SX 40 scanning electron microscope. The acceleration voltage was 10 kV and the magnification varied between 5000 \times and 15000 \times . A Philips EM-420T scanning transmission electron microscope was also used where higher magnifications were desired: 50000 \times and 100000 \times .

Fiber Tensile Strength

The fiber strength was measured in tension for various fiber gauge lengths: 10, 20, 27, 45 and 80 mm. Single filaments were attached to two aluminum tabs with a two-part epoxy adhesive. The distance between the tabs defined the gauge length. The upper tab had a hole which allowed it to be suspended under a PM 300 Mettler balance. The lower tab, that weighed only 0.22 g, was secured between the jaws of a microvise mounted on a vertical translator that moved at a speed of 5 $\mu\text{m}/\text{sec}$. Care was taken that no initial tension was applied to the filament prior to the test. The breaking force was recorded by a personal computer. The mean value, μ , of the tensile strength for a given gauge length and the standard deviation, σ , were calculated by assuming a 2-parameter Weibull distribution

$$f(x) = \begin{cases} abx^{b-1} e^{-ax^b} & (x > 0) \\ 0 & (x \leq 0) \end{cases} \quad (12)$$

$$\mu = \int_0^{\infty} xf(x) dx = a^{-1/b} \Gamma(1 + 1/b) \quad (13)$$

and

$$\begin{aligned} \sigma &= \left[\int_0^{\infty} (x - \mu)^2 f(x) dx \right]^{1/2} \\ &= a^{-1/b} [\Gamma(1 + 2/b) - [\Gamma(1 + 1/b)]^2]^{1/2} \end{aligned} \quad (14)$$

where $f(x)$ is the probability density function and the parameters "a" and "b" are computed by using a maximum likelihood approach, *i.e.* by solving:

$$\left. \begin{aligned} \frac{\partial L(a,b)}{\partial a} = 0 \\ \frac{\partial L(a,b)}{\partial b} = 0 \end{aligned} \right\} \Rightarrow \left\{ \begin{aligned} \frac{n}{b} + \sum_{i=1}^n \ln x_i - n \frac{\sum_{i=1}^n x_i^b \ln x_i}{\sum_{i=1}^n x_i^b} = 0 \\ a = \frac{n}{\sum_{i=1}^n x_i^b} \end{aligned} \right. \quad (15)$$

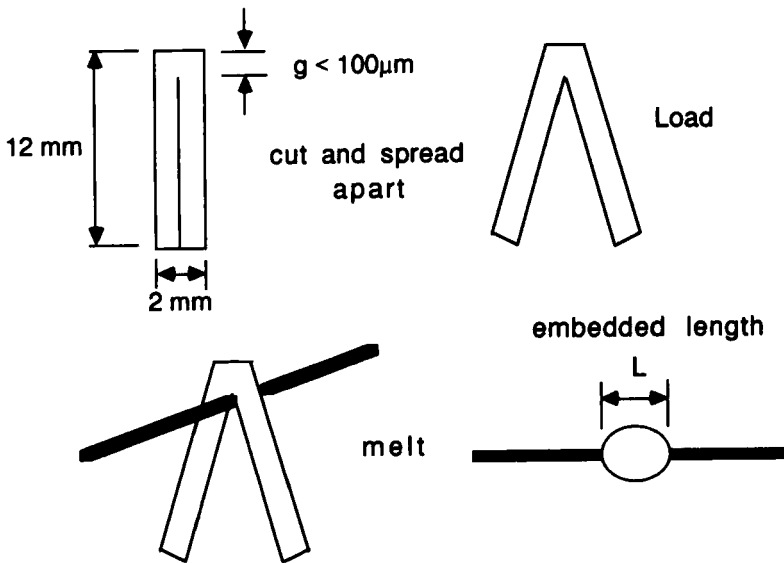


FIGURE 2 Schematic diagram of the sample preparation: deposition of a resin droplet on a single filament. (from Reference 15)

where L was the log likelihood function of the sample of “ n ” experimental measurements “ x_i .”

Microbond Pull-Out Test

The experimental procedure followed in this work has been described elsewhere¹⁵⁻¹⁹ and will be only briefly summarized here. Single fibers were laid across an aluminum fixture of rectangular donut shape. Small strips of polymer film were notched and put on the fibers as shown in Figure 2. The fixture was then introduced in a muffle furnace equilibrated at 454°C. A muffle furnace was necessary to reach the high temperatures required to melt the polymer used. In preliminary experiments it was observed that PES on IM7 carbon fibers did not melt completely when put in the furnace at 413°C for less than 15 minutes. However, initial furnace temperatures between 450 and 500°C proved to be optimal for the melting of PES in 2 minutes. The polymer strips (2 mm × 12 mm) were cut out of 75 μm thick extruded PES films (Stabar® S100) provided by ICI Films. All samples were prepared by melting the polymer strips in 2 minutes in the furnace at the initial temperature of 454°C. Figure 3 indicates that the actual temperature experienced by the samples does not exceed 370°C. The samples were subsequently quenched by rapid exposure to room temperature. These samples were referred to below as “quenched” or “Q.” After the initial quench (Q) some samples were re-heated for one hour in the furnace equilibrated at 240°C or 280°C. These samples were referred to as “annealed” or “A.” After annealing, the samples were either quenched a second time (Q’) by rapid cooling to room temperature or slowly cooled to room temperature in the

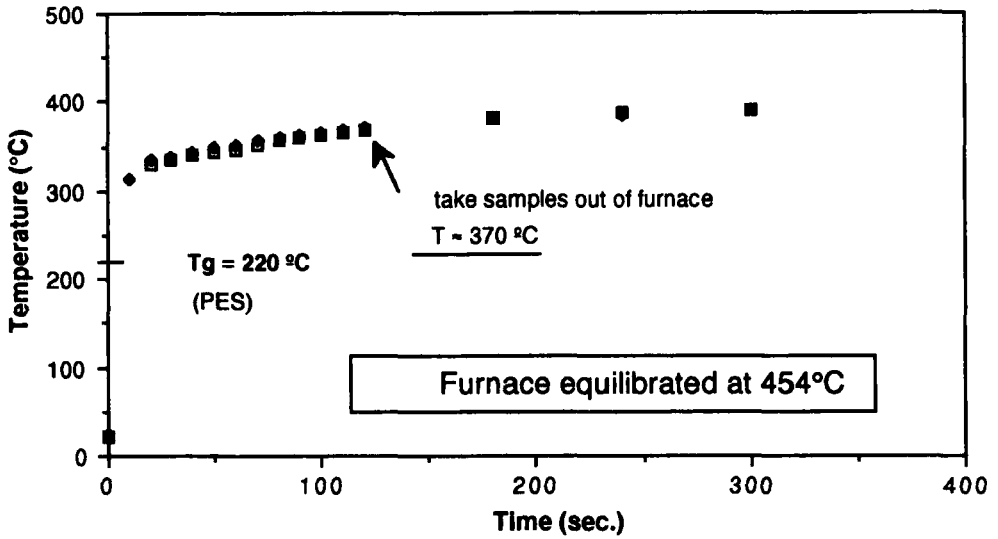


FIGURE 3 Sample temperature profile: temperature of the fibers and polymer as a function of time when the specimens are introduced into the muffle furnace equilibrated at 454°C.

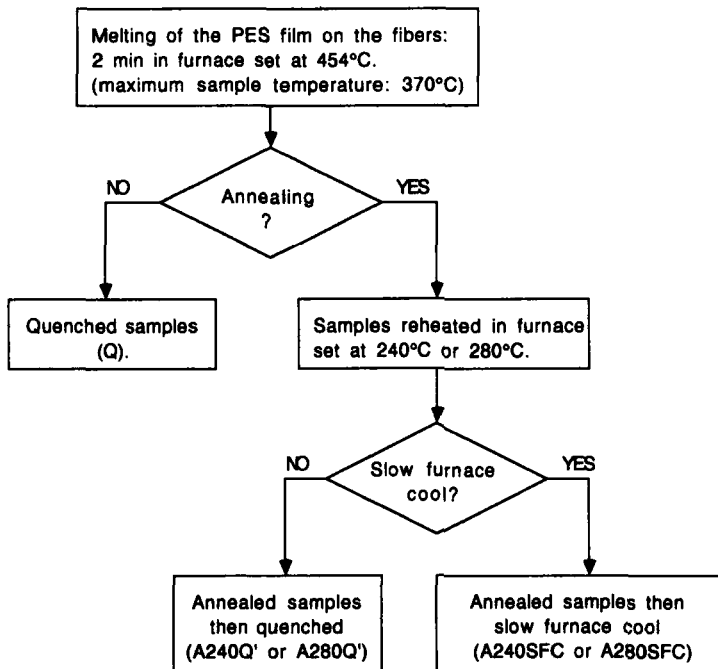


FIGURE 4 Annealing procedure flow chart.

muffle furnace (SFC or slow furnace cooling). The experimental procedure is summarized in the flow chart shown in Figure 4. In the following discussion, the above procedure will be referred to "annealing at 240°C or 280°C." It must be emphasized that these temperatures correspond to the equilibrium temperature of the furnace. It will be seen later that the actual temperature experienced by the samples is much lower. The sample temperature profiles are shown in Figures 16a and 16b.

The fiber was suspended under a Mettler PM 300 balance which was used to measure the debonding load. Each filament was attached to an upper tab as described for the fiber tensile strength test.

The samples were tested in shear in a custom-made microvise, as shown schematically in Figure 5. The microvise is fixed on a motorized stage that moved downward at 5 $\mu\text{m}/\text{sec}$. The readings were transmitted from the balance to a personal computer.

RESULTS AND DISCUSSION

Scanning Electron Microscopy

SEM photomicrographs of the IM7 carbon fibers show the smooth longitudinal striations resulting from the spinning process. The photographs do not indicate any appreciable roughening or dimensional changes, no matter which plasma treatment was used. The surface of the 2 min. air plasma treated fibers was identical in appearance to those of the as-received fibers. As a consequence, the value of 5.5 μm for the fiber diameter was used in all calculations. This value measured on SEM micrographs was in good agreement with results of wetting experiments made in n-hexane on as-received fibers: $5.3 \pm 0.5 \mu\text{m}$ (average of six samples).

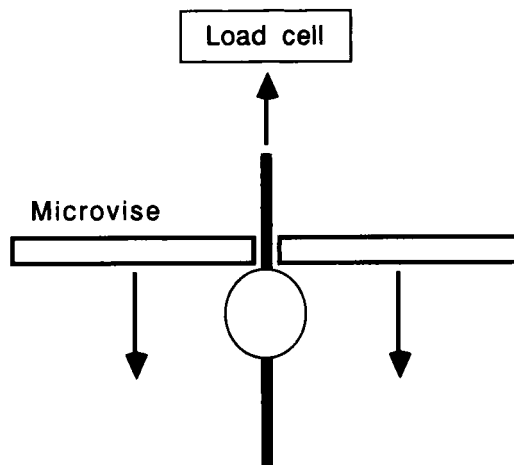


FIGURE 5 Schematic diagram of the microbond pull-out test.

TABLE I
XPS analysis of IM7 carbon fibers before and after plasma treatments.
Atomic concentrations expressed in percent

Plasma treatment	As-received	NH ₃ plasma (15 sec.)	Ar plasma (15 sec.)	Air plasma (15 sec.)
Carbon	85.0 ± 1.3	84.8 ± 0.7	79.5 ± 0.5	76.0 ± 2.2
Oxygen	9.9 ± 0.8	8.0 ± 0.3	15.8 ± 0.4	19.8 ± 1.2
Nitrogen	5.1 ± 0.6	7.2 ± 0.7	4.7 ± 0.1	4.1 ± 1.3

X-ray Photoelectron Spectroscopy

XPS analysis indicated that both argon and air plasmas increase significantly the surface oxygen content, as indicated in Table I. The oxidation of the surface of the fibers treated in an argon plasma was attributed to post-treatment reaction with atmospheric oxygen and water vapor as the fibers were exposed to air. This explanation was substantiated by the almost constant oxidation level, measured by the O/C ratio, as the treatment time was increased, as shown in Figure 6a. Traces (<1%) of sodium were observed on air plasma treated fibers but it was unclear whether the sodium comes from the wall of the plasma chamber or from within the bulk of the fiber. It was observed that the air plasma was the only treatment that increases significantly the fiber surface oxygen content with time. Figure 6b shows that the nitrogen content remains almost constant over time for both air and argon plasmas. In the case of an ammonia plasma, the nitrogen concentration reaches a plateau

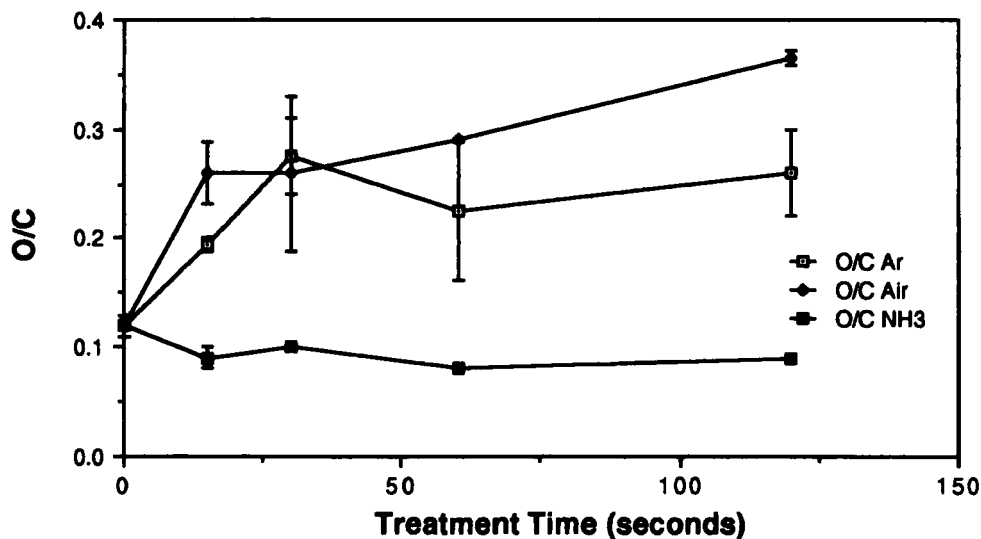


FIGURE 6a Influence of the treatment time on the fiber surface composition. Oxygen to carbon ratio of atomic concentrations obtained by XPS.

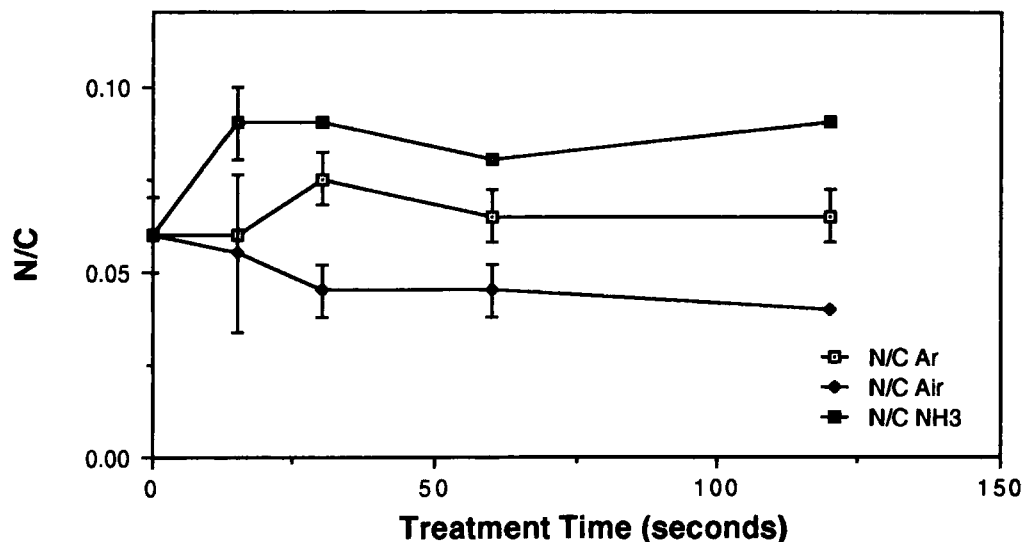


FIGURE 6b Influence of the treatment time on the fiber surface composition. Nitrogen to carbon ratio of atomic concentrations obtained by XPS.

after an initial increase. Except for the air plasma, any surface modification was completed within the first 15 seconds of the treatment.

Figures 7a and 7b show representative deconvoluted C1s spectra of as-received and ammonia plasma treated (15 sec.) fibers. The assignments of the curve fitted C1s peaks for as-received and plasma-treated fibers, based on literature data,²¹⁻²⁶

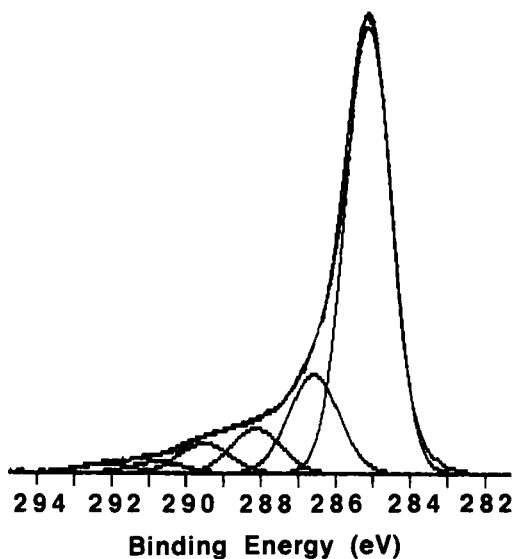


FIGURE 7a Carbon C1s curve-fitted spectrum of as-received fibers.

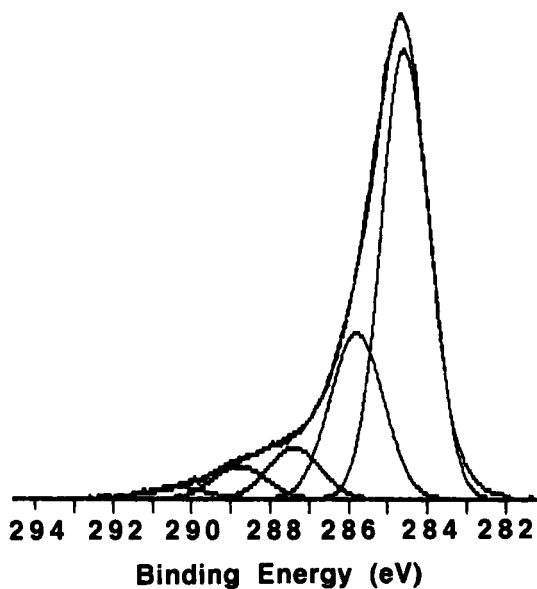


FIGURE 7b Carbon C1s curve-fitted spectrum of ammonia plasma treated (15 sec.) fibers.

are summarized in Table II. Although C—N and C=N species are expected to appear closer to the main carbon peak, C1, than C—O species, *i.e.* with a +1.0 eV shift instead of +1.5 eV, they have been assigned to the same portion, C2, of the C1s curve-fitted spectrum. XPS analysis of polymer films containing C—N and C=N moieties showed that these groups give rise to a C2 peak shifted at about +1.5 eV (from C1), similar to C—O groups. The goodness of the fit of the deconvoluted C1s spectra shown in Figures 7a and 7b suggests strongly that no significant peak can be fitted between the C1 and C2 peaks without reducing noticeably their FWHM. Table III shows that all plasma treatments reduce the overall importance of the main graphitic peak, C1. This observation explains, in part, the lower γ_s^d measured by contact angle, as noted in Table VI.

Argon and air plasmas treated fibers were characterized by high C4 and C5 peaks which explains the increase in surface polarity. The ammonia plasma increases the total nitrogen surface atomic concentration on the fibers. The deconvolution of the nitrogen N1s spectra obtained with as-received and ammonia plasma treated fibers

TABLE II
Identification of the peaks from a curve-fitted C1s spectrum

Curve fitted peak	C1	C2	C3	C4	C5
BE/chem. shift (eV)	285.0	≈ +1.5	≈ +3.0	≈ +4.5	≈ +6.0
Origin of the peak	C—C, C—H	C—O, C—N, C=N	C=O, N—C=O	O—C=O	O—CO—O, $\pi \rightarrow \pi^*$

TABLE III
Curve fitting of the XPS C1s spectra. Atomic concentrations expressed in percent of the total composition

Plasma treatment	As-received	NH ₃ plasma (15 sec.)	Ar plasma (15 sec.)	Air plasma (15 sec.)
C1	58.8 ± 0.8	50.8 ± 1.1	50.4 ± 4.2	42.5 ± 2.5
C2	13.1 ± 1.3	21.8 ± 1.7	16.5 ± 1.8	11.4 ± 0.3
C3	7.1 ± 0.6	6.4 ± 0.4	7.5 ± 1.2	8.2 ± 0.4
C4	4.2 ± 0.3	4.4 ± 0.1	5.0 ± 1.1	8.6 ± 0.5
C5	1.6 ± 0.2	1.4 ± 0.4	2.2 ± 0.4	3.9 ± 0.2

are very similar, as shown in Figures 8a and 8b as well as in Table IV. This suggests that the ammonia plasma did not create new nitrogen functionalities but enhanced the presence of those already present in or on the fibers through a "cleaning" process.

Tows of treated carbon fibers stored in a desiccator for two weeks (air plasma) or one month (ammonia plasma) were analyzed by XPS. The equivalence of the surface atomic composition of freshly treated fibers (D + 1day) with those of fibers treated and stored (D + 30days and D + 16days), see Table V, suggest that these treatments were very durable.

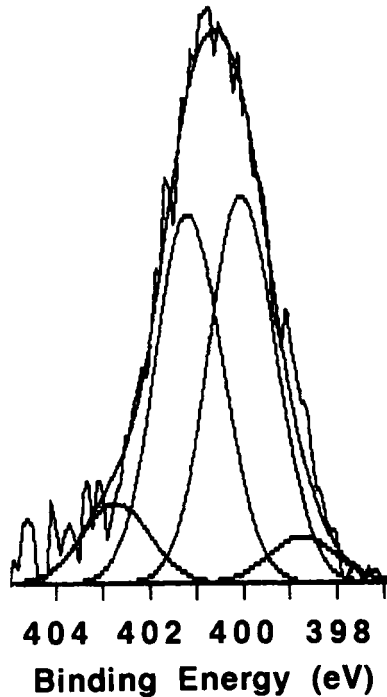


FIGURE 8a Nitrogen N1s curve-fitted spectrum of as-received fibers.

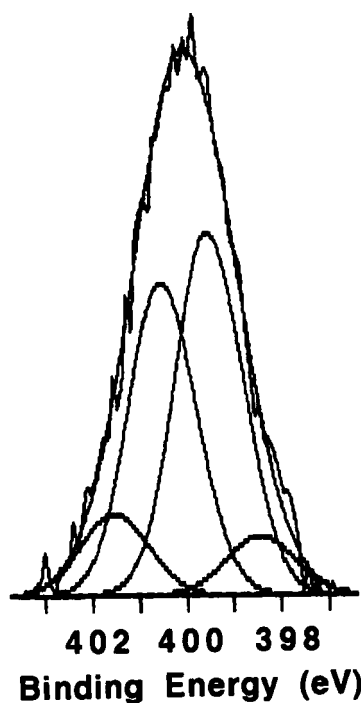


FIGURE 8b Nitrogen N1s curve-fitted spectrum of ammonia plasma treated (15 sec.) fibers.

TABLE IV
Curve fitting of the XPS N1s spectra. Atomic concentrations expressed in percent of the total nitrogen

Fiber surface treatment	As-received	NH ₃ plasma (15 sec.)
N1 (398.3–398.7 eV)	6.1 ± 0.5	6.8 ± 0.9
N2 (399.5–400.0 eV)	43.1 ± 4.4	43.3 ± 1.7
N3 (400.8–401.1 eV)	39.3 ± 2.9	39.2 ± 2.4
N4 (402.3–402.7 eV)	11.5 ± 1.3	10.6 ± 0.5

TABLE V
Durability of plasma treatments. Atomic concentrations expressed in percent

	Ammonia plasma		Air plasma	
	D+1 day	D+30 days	D+1 day	D+16 days
Carbon	85.1	85.0	78.0	78.2
Oxygen	7.9	8.3	18.6	18.2
Nitrogen	7.0	6.7	2.8	3.2
Sodium	/	/	0.6	0.4

DCA

Two characteristic traces observed during a contact angle experiment were reproduced in Figure 9a for as-received IM7 fibers and Figure 9b for argon plasma treated fibers.

The first step in the curves corresponds to the wetting of the fiber by the hydrocarbon. The force recorded by the electrobalance is related to the contact angle through the following equation:

$$f = p \gamma_L \cos(\theta) - B \approx p \gamma_L \cos(\theta) \quad (18)$$

where p is the fiber perimeter

γ_L is the n-alkane surface tension

θ is the contact angle

B is a buoyancy correction factor which is negligible for these small fibers.

Because the n-alkane wets the fiber completely, $\theta=0$ and the force measured depends only upon the surface tension of the solvent used. The perimeter was assumed to remain constant for all fibers.

Figure 9a shows a hysteresis loop during the second step in the case of the as-received fiber. The hysteresis phenomenon can be tentatively attributed to chemical heterogeneities on the fiber surface.²⁷ This section of the trace corresponds to the wetting of the fiber by the polar liquid, *i.e.* the formamide. The disappearance of the hysteresis after plasma treatment of the fiber seen in Figure 9b is due to better wetting of the formamide because of stronger non-dispersive interactions (see Table VI).

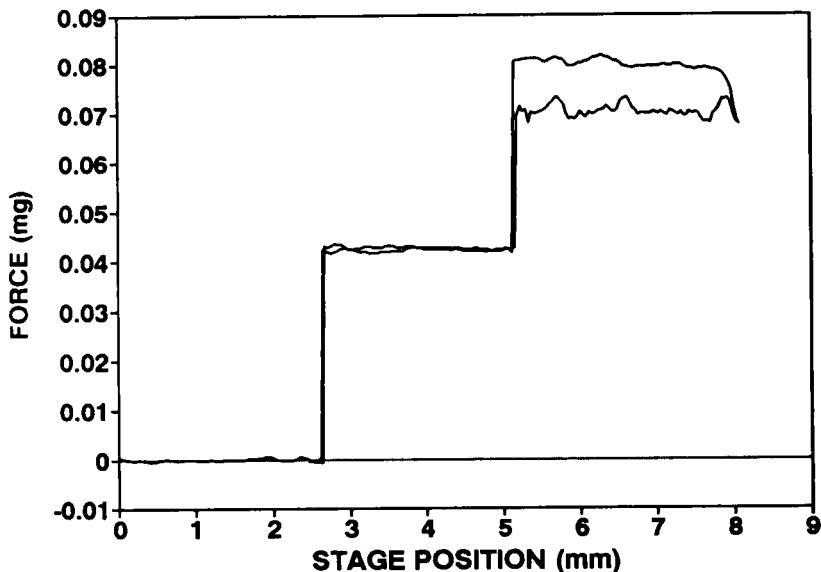


FIGURE 9a DCA trace of as-received IM7 carbon fibers immersed the n-hexadecane/formamide system.

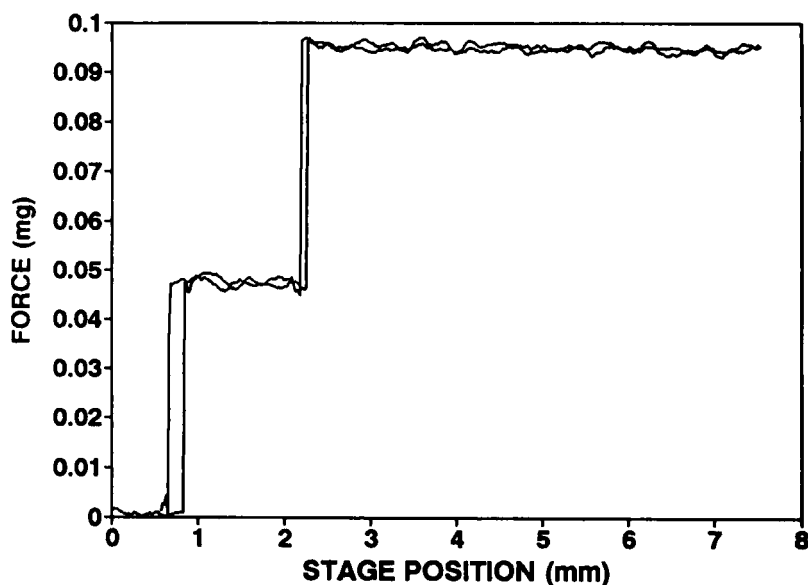


FIGURE 9b DCA trace of IM7 carbon fibers treated 15 sec in an argon plasma and immersed the n-hexadecane/formamide system.

Plots such as those reproduced in Figure 10, for as-received fibers, result from the application of equation (5) to various n-alkane/formamide systems, as described previously.

$$X = (\gamma_F^d)^{1/2} - (\gamma_H^d)^{1/2} \quad (19)$$

$$Y = \gamma_F - \gamma_H + T \quad (20)$$

The advancing and receding lines correspond to the advancing and receding contact angle traces, respectively. The slope of each line leads to the dispersive component, γ_s^d , while the intercept is equal to I_{SF}^p . Some authors calculate the polar term γ_s^p , from

$$I_{SF}^p = 2[\gamma_s^p \gamma_F^p]^{1/2} \quad (21)$$

This assumes that Fowkes' derivation for the dispersive interactions²⁸ applies also to non-dispersive interactions despite his own proof of the contrary.²⁹ Table VI summarizes the surface energy results.

All plasma treatments decrease γ_s^d and increase the non-dispersive interaction

TABLE VI
Surface free energy (in mJ/m^2) of IM7 carbon fibers before and after plasma treatment

Plasma treatment	As-received	NH_3 plasma (15 sec.)	Ar plasma (15 sec.)	Air plasma (15 sec.)
γ_s^d	49	41	11	11
I_{SF}^p	36	45	58	56

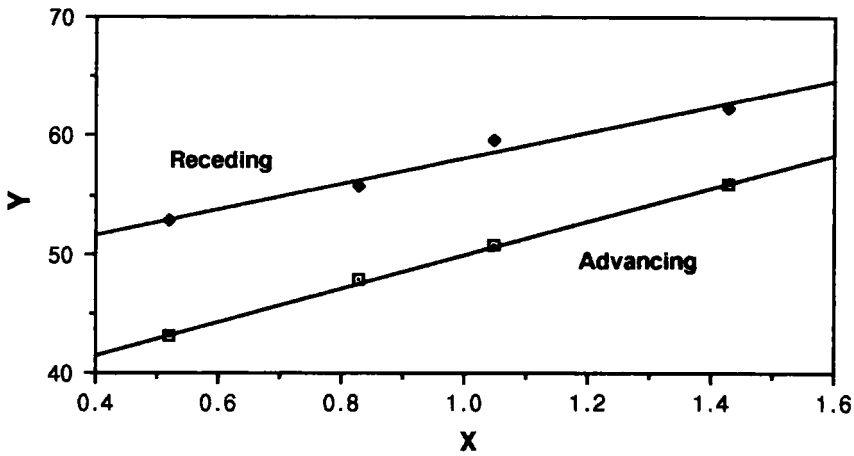


FIGURE 10 Advancing and receding curves calculated from equation (5).

term, I_{SF}^p . Argon and air plasmas give similar results for both γ_s^d and I_{SF}^p . The significant increase in the surface "polarity" due to the argon and air plasmas can be correlated to the corresponding increase in the surface oxygen content (see Table I) and, in particular, to the highest oxidized carbon functionalities, C4 and C5 as shown in Table III. The gain in surface "polarity" after ammonia plasma treatment can be correlated to the increase in the C2 peak.

Fiber Strength

It has been shown above that the plasma treatments used affected the surface chemistry and, therefore, the surface energy of the fibers. The surface morphology was not altered to any appreciable extent. The plasma treatments also have a significant effect on the fibers' strength. Figure 11 shows how the average tensile strength, μ ,

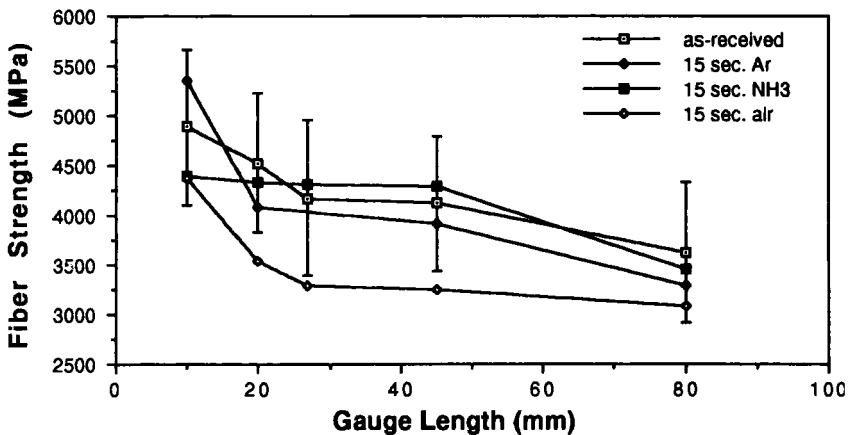


FIGURE 11 Variation of the fiber tensile strength (μ in MPa) versus gauge length (GL in mm), after different surface treatments.

varies with the gauge length, GL. It is expected that μ decreases as GL increases because of the higher probability of finding a flaw, or defect, big enough to initiate failure at longer lengths. Because of the large scatter in the data, only the overall trend was considered in this analysis. The error bars were shown only for as-received fibers in order to keep the graph readable. The length of each error bar was equal to 2σ .

The decrease in μ is most severe for the air plasma treatment. The highly oxidative air plasma creates a high concentration of defects of critical size not seen in high resolution SEM. All the curves seem to converge at high gauge lengths ($GL > 80$ mm) since then the probability of finding a critical size defect was close to 1, regardless of the fiber treatment.

Microbond Pull-Out Test

The microbond pull-out test was used in this study as a tool to compare the effect of different plasma treatments on the polymer (PES)/carbon fiber adhesion. It was not the authors' intention to interpret the results in terms of interfacial shear forces. The experimental procedure (PES melting temperature and time, and testing conditions) was the same for all treatments, therefore the results may be compared.

It must be emphasized that the amount of resin deposited on each fiber was of paramount importance to obtain a single symmetrical droplet. Any excess of polymer results, after melting, in the formation of a string of droplets as shown in Figure 12. Single droplets, such as the one shown in Figure 13, requires that "g," as noted in Figure 2, is less than $100 \mu\text{m}$.

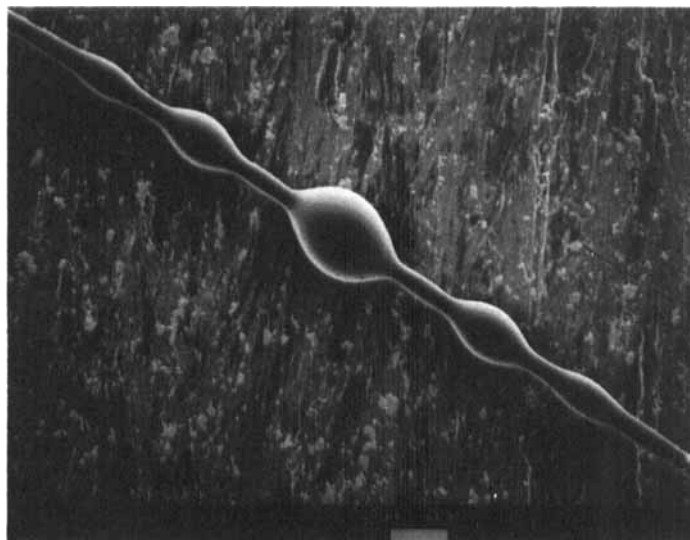


FIGURE 12 Scanning electron micrograph of a string of droplets of PES obtained when an excess ($g \approx 240 \mu\text{m}$, see Figure 2) of resin is deposited on the fiber.

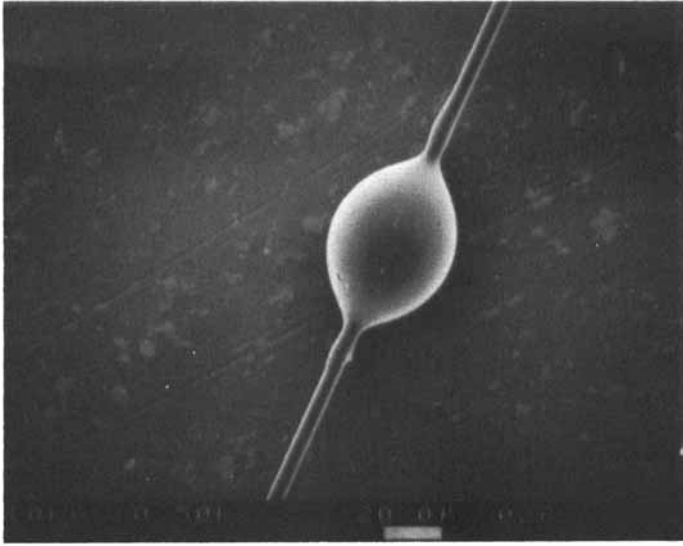


FIGURE 13 Scanning electron micrograph of a single droplet of PES obtained when a small ($g < 100 \mu\text{m}$, see Figure 2) amount of resin is deposited on the fiber.

Figure 14 shows the different types of debonding curves observed during the microbond pull-out experiments. Curves of type 1 were found to be associated with the slicing of the polymer droplets as well as, in some cases, the debonding with or without slicing of the droplet. The debonding loads (DL) observed with type 1 curves were usually smaller than the DL corresponding to other types of debonding

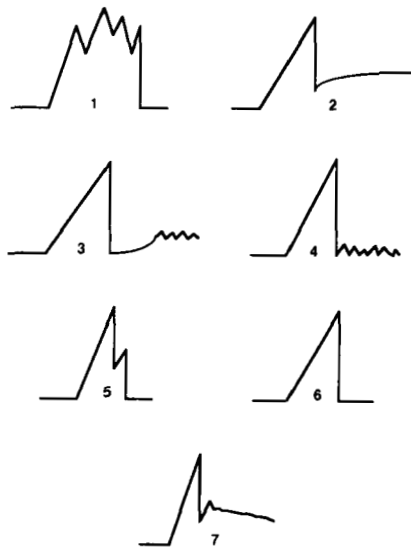


FIGURE 14 Schematics of the debonding curves observed during microbond pull-out experiments.

curves. No correlation was found between the debonding curves and the debonding loads or the mode of failure. It is interesting to note the variety of the shapes of the debonding curves, whereas other authors report only one typical pull-out curve.^{15,18,30,31}

SEM observations after pull-out testing showed little evidence of polymer left on the fibers. The analyzed spot size by XPS was too large for a surface analysis of single fibers after polymer debonding. It was, therefore, not possible to conclude positively that the failure occurs at the fiber/polymer interface.

The following results and discussion will focus only on samples which gave type 2-7 debonding curves, with the exclusion of type 1 because of the ambiguity concerning the slicing or debonding associated with this type. Figures 15a and 15b show that DL was independent of the size of the PES droplets as represented by the embedded length, L . This observation was true for all sets of data including more than 8 samples, regardless of the fiber surface treatment and annealing conditions. It can be seen also that, as a result of the experiment procedure followed, most values of L varied within a relatively short range, *i.e.* between 45 and 80 μm . This happened to be the case in all experiments, no matter what the fiber surface treatment or the annealing conditions of the PES droplets.

The mean values (± 1 standard deviation) of DL are reported in Table VII for the different fiber plasma treatments and polymer annealing conditions. The average DL of air and NH_3 plasma-treated fibers and quenched (Q) PES were greater than for non-treated fibers. An analysis of variance at the 95% confidence level³² (ANOVA95) indicates that the only significant difference between the means is between as-received and NH_3 plasma-treated fibers. The annealing process had a different effect on DL depending upon the fiber plasma treatment. Annealing at

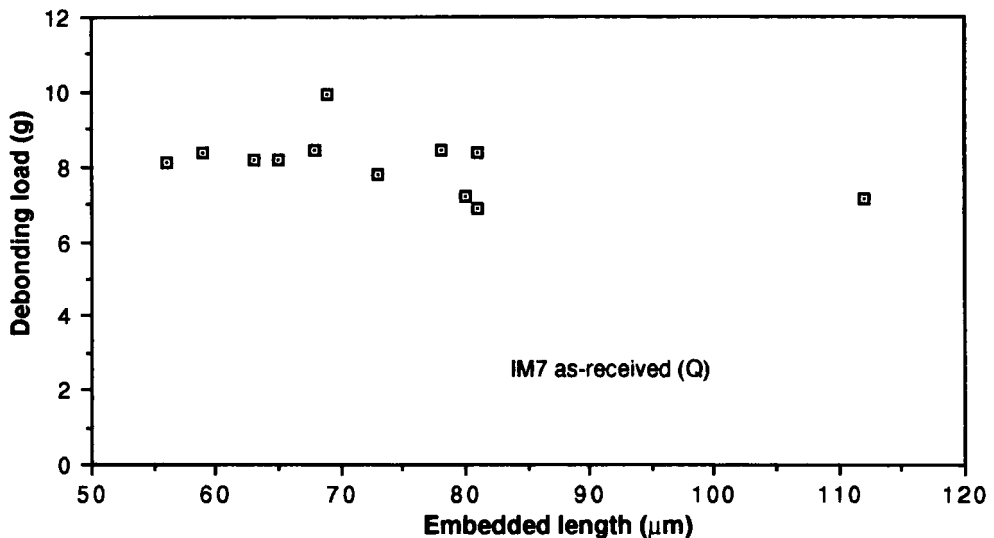


FIGURE 15a Variation of the debonding load (in grams) as a function of the droplet embedded length (in μm) for as-received IM7 carbon fibers and quenched PES.

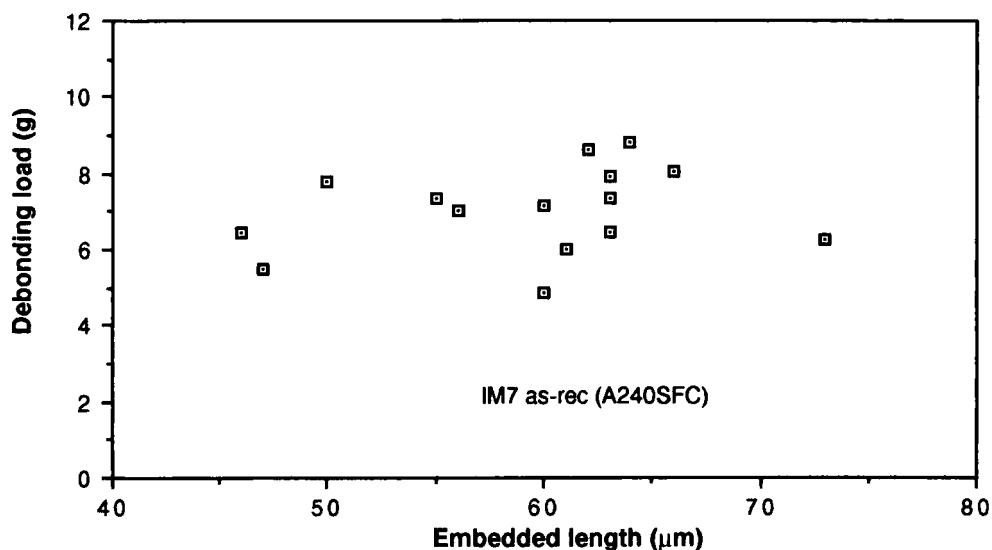


FIGURE 15b Variation of the debonding load (in grams) as a function of the droplet embedded length (in μm) for as-received IM7 carbon fibers and annealed PES (A240SFC).

240°C decreased DL of as-received samples (A240SFC) but annealing at 280°C (A280SFC) increased DL of the same samples compared with quenched samples (Q). An ANOVA95 tells us that the DL of A280SFC samples is significantly greater than the DL of both Q and A240SFC samples. Annealing had no effect on NH_3 plasma-treated fiber samples. Samples annealed at 240°C (A240SFC) showed no significant (ANOVA95) variation of DL depending on the fiber treatment, but if the annealing temperature was raised to 280°C (A280SFC) air plasma-treated fibers gave lower DL than as-received fibers. During the annealing at 240°C the samples were, in fact, heated only up to a maximum temperature of 224°C, as shown in Figure 16a, while the annealing at 280°C took the samples up to 260°C. A240SFC specimens were maintained at a temperature slightly above T_g for about 30 minutes. A280SFC specimens experienced a higher temperature for a longer period of time, about 100 min., as shown in Figure 16b.

The higher DL observed with as-received fibers samples annealed at 280°C can be

TABLE VII
Debonding load (in grams) as a function of the fiber surface treatment and the annealing conditions of the samples

Surface treat.→ annealing	As-received	Air plasma (15 sec.)	NH_3 plasma (15 sec.)
Q	8.1 ± 0.8	8.7 ± 1.0	9.4 ± 0.8
A240SFC	7.1 ± 1.0	7.2 ± 1.3	8.4 ± 0.5
A280SFC	9.2 ± 1.1	7.8 ± 0.7	8.6 ± 0.5
A280Q'	8.2 ± 0.6	nd	nd

nd: not determined.

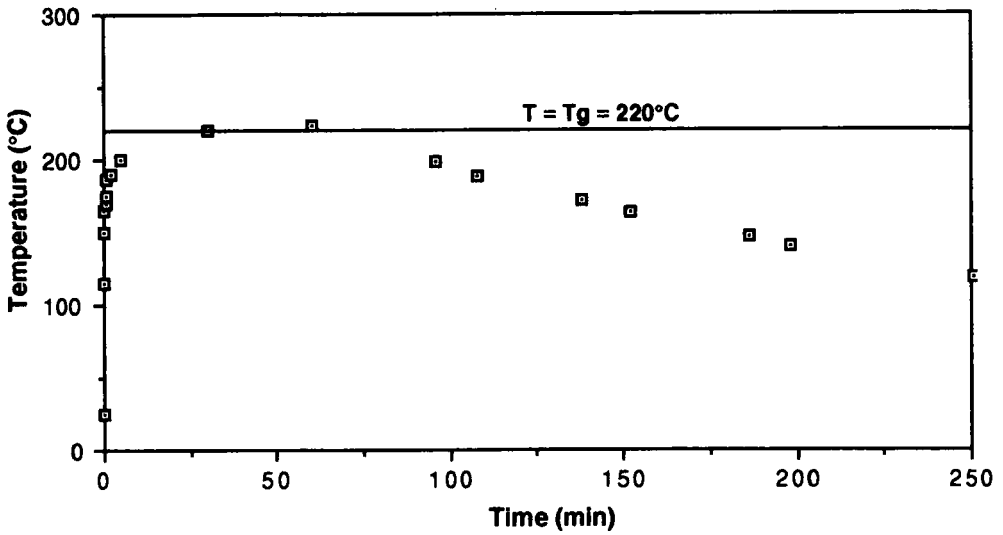


FIGURE 16a Temperature profile of the samples during a one-hour annealing at 240°C.

explained by the fact that in this condition the polymer is re-heated at a temperature significantly above its T_g . The PES molecules can minimize their energy state by adopting "preferred low energy adsorbed conformations." The comparison of A280SFC and A280Q' samples for as-received fibers indicates that the more time the polymer chains are held at a temperature above T_g the greater the adhesion. In the case of NH_3 plasma-treated fibers the PES molecules must have anchored themselves in adsorbed conformations which maximized the work of adhesion

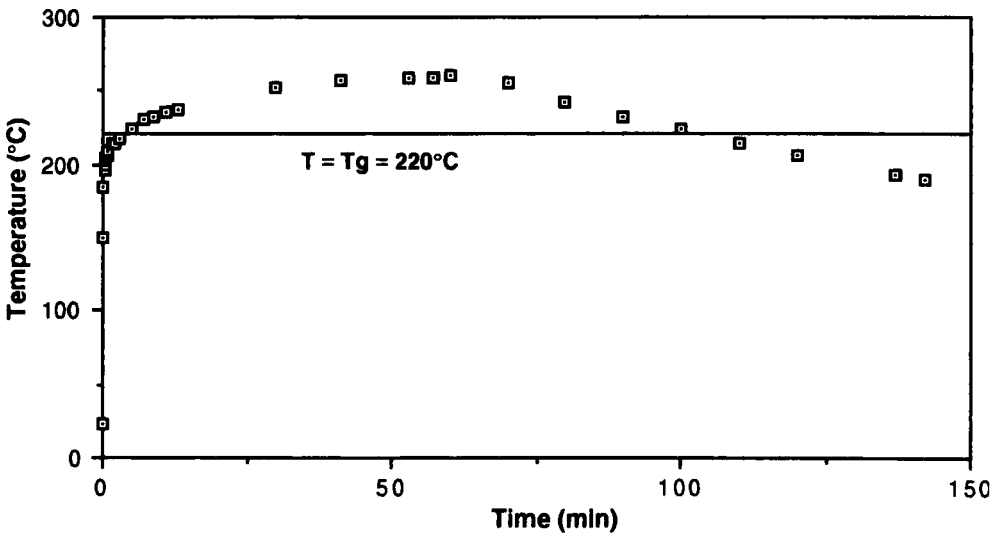


FIGURE 16b Temperature profile of the samples during a one-hour annealing at 280°C.

during the melting step that led to the formation of the droplets. The additional thermal energy put into the fiber/matrix system during the annealing stage had no further effect on the adhesion. Bulk shrinkage may occur as a result of the annealing but it cannot explain by itself the increase in adhesion observed with as-received fibers. If shrinkage were the only mechanism, air- and NH_3 plasma-treated fibers should also show a stronger adhesion to PES when the samples are annealed at 280°C .

The lack of sufficient data corresponding to smaller L ($L < 40\mu\text{m}$) and to larger L ($L > 80\mu\text{m}$) precludes further interpretation of the results.

CONCLUSION

Plasma treatments have been used successfully to modify the energetics of carbon fibers surface by either introducing specific functional groups onto the surface of the fibers (air and argon plasmas) or "cleaning" the surface (NH_3 plasma). It was found that the plasma effect was obtained very rapidly, in less than 15 seconds, and that the plasmas did not modify the surface morphology to any appreciable extent but that the fiber strength was affected. The microbond pull-out test has been used effectively to determine the influence of plasma treatments and annealing on the adhesion between PES and IM7 carbon fibers. It has been shown that an annealing treatment of the polymer droplets at a temperature high enough above T_g can improve the polymer/fiber adhesion for untreated fibers. It was found that in the case of IM7 carbon fibers and PES the ammonia plasma treatment enhanced the adhesion of quenched samples.

Acknowledgements

The authors wish to acknowledge the financial support of the Virginia Institute for Material Systems and the National Science Foundation Science and Technology Center at Virginia Tech. We thank Dr. B. Miller and Dr. U Gaur for their help in starting the microbond pull-out test. Dr. R. A. Latour is gratefully thanked for his most helpful suggestions about the droplet formation. We thank Mr. F. Webster, Dr. N. Eiss and Dr. D. Dillard for their useful comments during the process of this work. We thank Mr. F. Cromer for his teaching of the use of the XPS and SEM, as well as the physics shop, the electronics shop and the glass shop, at Virginia Tech, for building many of the experimental devices used in this research. The help of Dr. K. Ye in the statistical analysis and interpretation of the data is appreciated.

References

1. Committee on thermoplastic composite and structural components, "The place for the thermoplastic composites in structural components," Final Report, NMAB-434, National Academy Press 1987.
2. J. B. Donnet and R. C. Bansal, in *Carbon Fibers*, 2nd ed. Marcel Dekker, Inc., New York and Basel, 1990, p. 187.
3. J. B. Donnet, M. Brendle, T. L. Dhami and O. P. Bahl, *Carbon* **24**(6), 757 (1986).
4. C. Jones and E. Sammann, *Carbon* **28**(4), 509 (1990).
5. *Ibid.*, p. 515.
6. S. P. Wesson and R. E. Allred, in *Inverse Gas Chromatography*, Lloyd Schreiber, Ward, Eds., *ACS Symposium Series* **391** (Am. Chem. Soc., Washington, D.C., 1988), p. 203.
7. A. Bolvari and T. C. Ward, in *Inverse Gas Chromatography*, Lloyd Schreiber, Ward, Eds., *ACS Symposium Series* **391** (Am. Chem. Soc., Washington, D.C., 1988), p. 217.

8. S. P. Wesson and R. E. Allred, *J. Adhesion Sci. Technol.*, **4**(4), 227 (1990).
9. J. B. Donnet, J. Schultz and K. Tsutsumi, *Proc. 4th Intern. Conf. on Chem. Thermodynamics, Montpellier (FRANCE)*, **7**, 126 (1975).
10. J. Schultz, K. Tsutsumi and J. B. Donnet, *J. Colloid and Interface Science* **59** (2), 272 (1977).
11. *Ibid.*, p. 277.
12. J. Schultz, C. Cazeneuve, M. E. R. Shanahan and J. B. Donnet, *J. Adhesion* **12**, 221 (1981).
13. J. B. Donnet and R. C. Bansal, in *Carbon Fibers*, 2nd ed. (Marcel Dekker, Inc., New York and Basel, 1990), p. 305.
14. M. E. R. Shanahan, C. Cazeneuve, A. Carré and J. Schultz, *J. Chim. Phys.* **79**(3), 241 (1982).
15. B. Miller, P. Muri and L. Rebenfeld, *Comp. Sci. Tech.* **28**, 33 (1987).
16. G. P. Desio, B. Miller and L. Rebenfeld, *Proc. AIChE Annual Meeting*, Washington, D.C., November, 1988.
17. B. Miller and U. Gaur, *J. Adhesion* **29**, 103 (1989).
18. U. Gaur and B. Miller, *Comp. Sci. Tech.* **34**, 35 (1989).
19. U. Gaur, G. Desio and B. Miller, *Plastic Engineering*, October, 1989, p. 43.
20. R. A. Latour Jr., J. Black and B. Miller, *J. Mater. Sci.* **24**, 3616 (1989).
21. A. Proctor and P. Sherwood, *J. Electron Spectroscopy and Related Phenomena* **27**, 39 (1982).
22. A. Proctor and P. Sherwood, *Carbon* **21**(1), 53 (1983).
23. C. Mozlowski and P. Sherwood, *J. Chem. Soc., Faraday Trans. 1*, **80**, 2099 (1984).
24. C. Kozlowski and P. Sherwood, *J. Chem. Soc., Faraday Trans. 1*, **81**, 2745 (1985).
25. C. Kozlowski and P. Sherwood, *Carbon* **24**(3), 357 (1986).
26. G. Guilpain, Ph.D. dissertation, "Etude de traitements superficiels de fibres de carbone par voie électrolytique", Université de Haute Alsace, 1988.
27. L. S. Penn and B. Miller, *J. Colloid Interface Sci.*, **78**, 238 (1980).
28. F. M. Fowkes, *Ind. Eng. Chem.* **56**(12), 40 (1964).
29. F. M. Fowkes, *J. Adhesion* **4**, 155 (1972).
30. M. R. Piggott, A. Sanadi, P. S. Chua and D. Andison, *Proc. Int. Conf. on Comp. Interfaces*, H. Ishida and J. L. Koenig, Eds. (Elsevier, New York, 1986), p. 109.
31. M. R. Piggott and S. R. Dai, *Polym. Eng. Sci.* **31**(17), 1246 (1991).
32. Abacus Concepts, StatView II. (Abacus Concepts, Inc., Berkeley CA, 1987).